iopscience.iop.org

Home Search Collections Journals About Contact us My IOPscience

A batch-mode micromachining process for spherical structures

This content has been downloaded from IOPscience. Please scroll down to see the full text.

2014 J. Micromech. Microeng. 24 025002

(http://iopscience.iop.org/0960-1317/24/2/025002)

View the table of contents for this issue, or go to the journal homepage for more

Download details:

IP Address: 141.213.9.154
This content was downloaded on 26/01/2015 at 16:34

Please note that terms and conditions apply.

IOP Publishing Journal of Micromechanics and Microengineering

J. Micromech. Microeng. **24** (2014) 025002 (8pp) doi:10.1088/0960-1317/24/2/025002

A batch-mode micromachining process for spherical structures

Tao Li[1], Karthik Visvanathan[2] and Yogesh B Gianchandani

Center for Wireless Integrated MicroSensing and Systems (WIMS^2), University of Michigan, Ann Arbor, MI, USA

E-mail: litz@umich.edu

Received 25 August 2013, revised 14 November 2013
Accepted for publication 18 November 2013
Published 23 December 2013

Abstract

This paper reports a self-aligned three-dimensional process (3D-SOULE) that incorporates batch-mode micro ultrasonic machining (μUSM), lapping and micro electro-discharge machining (μEDM) for fabrication of concave and mushroom-shaped spherical structures from hard and brittle materials. To demonstrate the process, 1 mm structures are fabricated from glass and ruby spheres. The μEDM technique is used to create the tool for μUSM from stainless steel spheres. Stainless steel 440, which provides a tool wear ratio <5%, is chosen as the tool material. A 2 × 2 array is used for batch processing. For an ultrasound generator frequency of 20 kHz and a vibration amplitude of 15 μm, machining rates of 24 and 12 μm min^{-1} are obtained for glass and ruby spheres, respectively. An approximate linear relationship is observed between the measured roughness (R_a) of the machined surface and the product of the fracture toughness (K_{IC}) and the hardness (H) of the workpiece material ($K_{IC}{}^{3/2}H^{1/2}$).

Keywords: spherical microstructures, micro ultrasonic machining, 3D micromachining, glass micromachining, ruby micromachining

(Some figures may appear in colour only in the online journal)

1. Introduction

Three-dimensional (3D) microstructures in hemispheric, 'wine-glass' or mushroom shapes are attractive for certain types of inertial sensors and optical elements (figure 1) [1–4]. Most conventional surface and bulk microfabrication methods such as etching, film deposition and photolithography are limited to creating planar structures. Microfabrication methods, such as LIGA (a German acronym for lithography, electroplating and molding) [5, 6] and deep reactive ion etching (DRIE) [7, 8], are well suited for creating high-aspect-ratio structures out of metal and silicon, respectively. However, these methods are not easily adapted for making spherical shapes, and the material options are limited.

A number of 3D microfabrication efforts have utilized isotropic processes. The use of isotropic wet etching, deposition and oxidation to microfabricate free standing spherical structures from thermally grown silicon dioxide was discussed in [9]. A similar process that was recently reported used isotropic SF$_6$ plasma etching instead of wet silicon etching in the fabrication of anchored micro-hemispherical SiO$_2$ thin shells [10, 11]. The fabrication of dome-shaped structures utilizing the buckling of pre-stressed thin polysilicon films was discussed in [12]. Hemispherical thin shells made from sputtered ultra-low-expansion glass were formed using precision ball lenses as molds [13]. Thin film diamond hemispherical shells were made by chemical vapor deposition onto silicon molds formed using micro electro-discharge machining (μEDM) and isotropic wet chemical polish [14]. The thicknesses of the shells fabricated using these techniques have been limited to few microns.

Techniques based on thermally reflowing/forming of materials have also been reported. A blow molding technique has been used to make 3D shells by thermoplastic forming of bulk metallic glasses [15]. A wafer-scale glassblowing process has been reported for the fabrication of spherical shells from Pyrex® or ultra-low-expansion titania silicate glass composites [16, 17]. A half-toroid shell has been made from fused silica sheet by reflowing into a graphite mold; a blow torch provided

---

[1] Author to whom any correspondence should be addressed.

[2] Present Address: Intel Corporation, Chandler, AZ, USA.

0960-1317/14/025002+08$33.00

© 2014 IOP Publishing Ltd Printed in the UK

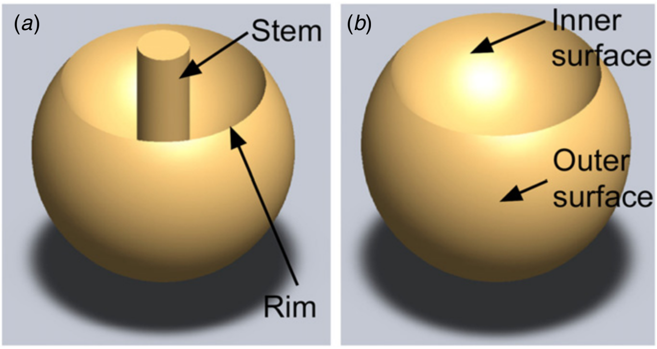

Figure 1. Schematics of: (*a*) mushroom-shaped and (*b*) concave spherical structures fabricated using the 3D-SOULE process.

localized heating with temperature beyond the melting point of the material [18]. High temperature equipment is needed for these techniques, and the required temperature can vary significantly for different materials. The structures usually have thermally induced residual stress that needs to be relieved by annealing. The structural geometry is typically in thin shell form due to the increased difficulty in reflowing of bulk material.

This paper reports a complementary method for integrating and micromachining concave and mushroom-shaped spherical structures from materials such as glass and ruby/sapphire[3]. Named 3D-SOULE, this is a 3D-capable and self-aligned process combining batch-mode micro ultrasonic machining (μUSM), lapping and μEDM.

Conventional USM has been widely accepted as an effective machining technique for hard and brittle materials, including most of the commonly used materials for high quality factor (Q) resonators [20]. We have previously reported a batch-mode μUSM process that can transfer lithographic patterns onto Macor® glass mica ceramic, lead zirconate titanate (PZT), quartz crystal and Zerodur® low-thermal-expansion glass ceramic [21, 22]. Planar or multi-level patterns with lateral feature sizes $\geqslant 25\ \mu$m and machining rates $>24\ \mu\text{m min}^{-1}$ have been demonstrated. Since this process does not involve any chemical processing or high temperature steps, it is possible to create stress-free structures in a wide variety of materials. No high-stress deformation is produced at or below the workpiece surface, and no thermal or chemical alteration is caused in the subsurface characteristics [20].

In the following sections, the details of the 3D-SOULE process are described in section 2. The process was demonstrated by fabricating concave and mushroom-shaped structures from N-BK7 glass and ruby spheres, and the fabricated mushroom structures were subjected to preliminary resonance characterization. Different tool material options were also assessed. The experimental results of the fabrication and the resonance characterization are reported in section 3, and are followed by discussion in section 4.

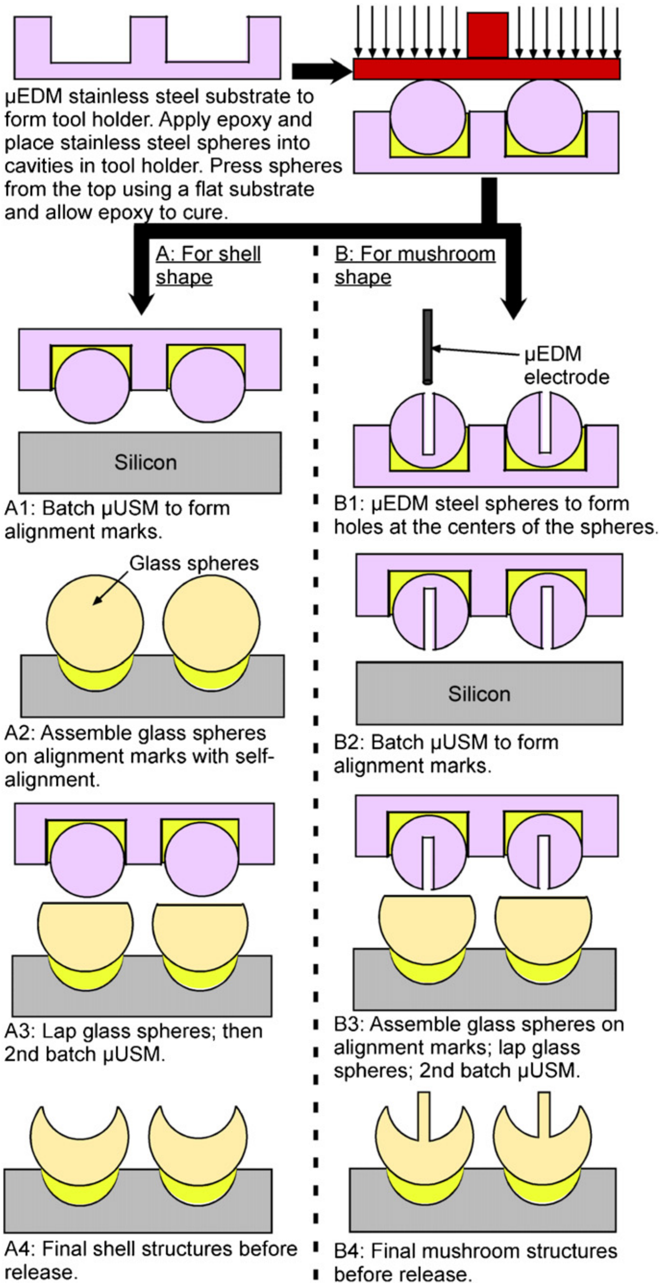

μEDM stainless steel substrate to form tool holder. Apply epoxy and place stainless steel spheres into cavities in tool holder. Press spheres from the top using a flat substrate and allow epoxy to cure.

A1: Batch μUSM to form alignment marks.

A2: Assemble glass spheres on alignment marks with self-alignment.

A3: Lap glass spheres; then 2nd batch μUSM.

A4: Final shell structures before release.

B1: μEDM steel spheres to form holes at the centers of the spheres.

B2: Batch μUSM to form alignment marks.

B3: Assemble glass spheres on alignment marks; lap glass spheres; 2nd batch μUSM.

B4: Final mushroom structures before release.

Figure 2. 3D-SOULE process flow diagram for fabrication of concave and mushroom-shaped spherical structures. 3D-SOULE process utilizes μEDM, μUSM and lapping to fabricate devices in the shapes mentioned above. This process can be applied to a wide variety of glasses, fused quartz, etc.

2. Process description

2.1. Process details

The concept of the 3D-SOULE process for fabricating concave and mushroom-shaped spherical structures is illustrated in figure 2. Initially, μEDM is used to micromachine cavities in a steel substrate for holding stainless steel spheres. This can be done in a serial manner by using a rotating tungsten rod as the tool electrode to scan or scroll on the workpiece surface. This method is appropriate for rapid prototyping because it does not require photolithographic masks. Alternatively, batch-mode μEDM can provide high throughput; multiple parts can be machined in parallel by using a high-aspect-ratio silicon electrode with patterns defined by DRIE [23]. In either case, the tool electrode and the stainless steel workpiece are immersed in dielectric oil (kerosene). Sequential spark microdischarges between the tool electrode (cathode) and the workpiece (anode) are fired, and material removal occurs by melting and evaporation with the thermal energy released during the discharge. This technique can be applied to any conductive material, including all metals and alloys, with reported lateral feature sizes $\geqslant 5\ \mu$m.

---

[3] Portions of this paper appear in conference abstract form in [19].

Nonconductive epoxy is applied into the cavities on the stainless steel substrate. Commercially available stainless steel spheres with high geometrical precision are then assembled into these cavities. These spheres are pressed into the epoxy from above using a flat substrate, after which the epoxy is allowed to cure. This ensures that the tips of all the spheres are at the same level (figure 2). For machining the mushroom shape, an additional μEDM step is performed to form cavities at the center of each of the stainless steel spheres (figure 2, step B1). This enables the formation of the stems for the mushroom-shaped structures. The diameter of the cavities determines the diameter of the stem in the mushroom-shaped structure at the end of the process, and the cavity depth should be larger than the desired height of the mushroom stem plus any tool wear during the μUSM step that forms the mushroom structure. The X–Y resolution of the positioning stage on the μEDM machine (Smaltec EM203) is 0.1 μm, which enables the fabrication of stainless steel spheres with centered holes. This completes the preparation of the stainless steel tool for batch-mode μUSM.

Next, the assembled stainless steel tool is used in batch-mode μUSM to form an array of shallow alignment marks on a silicon carrier substrate (figure 2, step A1 or B2). These alignment marks are used for assembly and self-alignment of the workpiece spheres on the carrier substrate, and have a depth that allows the spheres to rest on the circumferences of the circular marks.

This batch-mode μUSM technique is performed with a customized setup, which is currently capable of die-scale micromachining and can be migrated to wafer scale in the future [21, 22]. The stainless steel tool, which is vibrated by an ultrasound generator, is advanced toward the carrier substrate. Water-based slurry with ultrafine abrasive particles is supplied between the tool and the substrate. On the downward stroke of the vibration, the tool tip imparts energy to the particles, which, in turn, bombard and remove material from the substrate. The machined cavity shape is conformal to the tool tip. An in-process monitoring technique based on acoustic emission sensing, is used to monitor the acoustic vibrations generated during material removal, thus providing feedback control of the machining progress [22]. For machining the mushroom shape, an additional step is performed after batch-mode μUSM to remove the posts formed at the centers of the alignment marks.

Spheres of selected workpiece material, such as glasses, with high geometrical precision and high surface finish are mounted and self-aligned into the alignment marks created on the silicon carrier (figure 2, step A2 or B3). This ensures that the center of the tool spheres and the workpiece spheres are self-aligned to each other with high geometrical precision. The workpiece spheres are bonded to the silicon substrate using epoxy. Lapping is performed using abrasive slurry with ultrafine diamond powder to remove the excess epoxy and, optionally, to reduce the height of the workpiece spheres as desired (figure 2, step A3 or B3).

A second batch-mode μUSM on the lapped workpiece spheres is then performed to form the desired concave and mushroom-shaped spherical structures. The μUSM process leads to the formation of sharp edges along the rim of the fabricated structures. An additional lapping step can be performed in order to remove the sharp edges on the machined workpiece spheres. The machined workpiece is finally released from the silicon substrate using an appropriate solvent. Details are provided in section 3. Alternatively, these spheres can be mounted/bonded onto another device substrate for further handling/integration.

2.2. USM of brittle materials

As described in the section above, material removal during batch-mode μUSM occurs through the bombardment of energized abrasive particles on the workpiece. USM, including μUSM, is best suited for hard and brittle materials. It is easier to fracture these materials with a high local stress (i.e. microchipping) than to plastically deform them. For a fine particle with a mass m and a velocity v when it reaches the workpiece surface, the average force F_s that the particle exerts on the surface can be approximated as $F_s = 2mv/t_s$, where t_s is the contact time between the particle and the workpiece. For hard materials, t_s is very short, resulting in a significant force F_s. A high local stress is generated given the small contact area determined by the particle size, causing microchipping of the brittle workpiece. Because of the microchipping process, USM produces little or no damage or high-stress deformation at or below the surface [20].

The mass removal rate of the USM process can be affected by many parameters, including tool vibration amplitude (A) and frequency (f), static loading force (P) between the workpiece and the tool tip, fracture toughness (K_{IC}) and hardness (H) of the workpiece material, average size (d) and material properties of the abrasive particle. Many models of the mass removal rate have been developed for USM [20, 24, 25]. A simplified model for estimating material removal rates for stationary (non-rotary) USM is given by [25]

$$V \propto \frac{P^2}{K_{IC}^{3/2} H^{1/2}} \frac{f}{n}, \qquad (1)$$

where n is the effective number of particles between the tool tip and the workpiece. The mass removal rate increases with a larger f, a larger P, a smaller K_{IC} and H, and a larger d.

The post-USM surface roughness is affected by all parameters listed above. Arguably the most significant parameters are the size of the abrasive particles, the material properties of the workpiece and the particles, and the machining load. Although other models exist, it has been shown that the roughness (R_a) of machined surfaces

Table 1. Selected material properties and measured surface roughness (R_a) of machined surfaces.

Material	Fracture toughness K_{IC} (MPa · m$^{1/2}$)	Vickers hardness H (GPa)	Young's modulus E (GPa)	$10^{13}\ K_{IC}{}^{3/2}H^{1/2}$	Mean surface roughness R_a (μm)
N-BK7 glass [30–32]	0.85	7.5	82	6.787	0.476
Ruby/sapphire [30, 33–36]	2.10	22.6	345	45.749	0.019
Silicon (1 0 0) [37–39]	0.91	11.4	130	9.269	0.405
Macor® [40, 41]	1.53	3.9	66.9	11.819	0.400

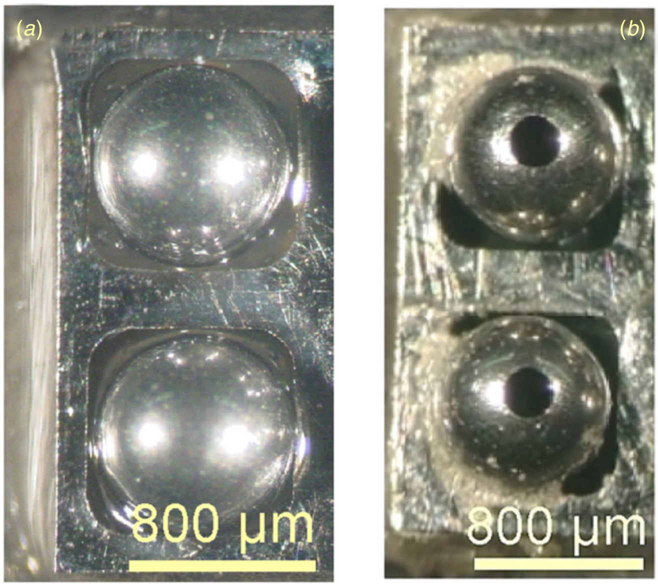

Figure 3. Photos of: (*a*) USM tool for fabrication of spherical shells. (*b*) USM tool with cavities at the center of the spheres for fabrication of mushroom-shaped structures.

has an approximate linear relationship with the product $K_{IC}{}^{3/2}H^{1/2}$ when other machining conditions remain the same [26]. Workpiece material with a larger product is expected to show a lower surface roughness, thus better surface finish. The relevant properties of the materials used in this process are listed in table 1.

3. Experimental results

3.1. Process characterization

The 3D-SOULE process was used to fabricate concave and mushroom-shaped structures from N-BK7 optical glass and ruby spheres. Commercially obtained high precision stainless steel spheres of 0.8 mm diameter (A.F.B.M.A. grade 25, Salem Specialty Ball Company, CT, USA), with high geometrical precision (sphericity <0.625 μm), were assembled into the cavities made by μEDM on the tool holder substrate to form the stainless steel tool. A 2 × 2 array of the tool spheres was used to demonstrate the batch processing capability. For machining the mushroom shape, an additional μEDM step created cavities of 200 μm diameter and 750 μm depth at the center of each of the stainless steel spheres. This was used to form a stem of ≈200 μm diameter on the mushroom-shaped structure. Figures 3(*a*) and (*b*) show the photographs of the assembled μUSM tools for fabrication of concave and mushroom-shaped spherical structures, respectively.

Table 2. Machining parameters for the batch-mode μUSM process used in the 3D-SOULE process.

Ultrasound generator frequency	20 kHz
Ultrasound vibration amplitude	15 μm
Abrasive powder (WC) avg. size	0.5–1 μm
Machining load	≈0.5 N
Avg. machining rate (depth); N-BK7	24 μm min^{-1}
Avg. machining rate (depth); ruby	12 μm min^{-1}
Cutting depth; N-BK7 glass	350 μm
Cutting depth; ruby	50 μm

Table 3. Comparison of tool wear in SS316 and SS440 spheres during μUSM process. The wear ratio is the ratio of the tool volume worn to the machined workpiece volume.

	SS316	SS440
Substrate machined	N-BK7 glass	N-BK7 glass
Depth of machining	300 μm	300 μm
Tool wear (volume)	1.30×10^{-11} m^3	3.68×10^{-12} m^3
Wear ratio	31.7%	4.46%

The assembled stainless steel tool was then used in batch-mode μUSM to form an array of 100 μm deep alignment marks on a silicon carrier substrate. The parameters used in μUSM are listed in table 2. A 20 kHz ultrasound generator with vibration amplitude of ≈15 μm was used. The particles were tungsten carbide powder of 0.5–1 μm diameter. For the mushroom shape, the post formed at the center of each alignment mark was manually removed. Other techniques such as DRIE can be used as well. A 2 × 2 array of mirror-finished N-BK7 glass spheres of 1 mm diameter and 0.625 sphericity (A.F.B.M.A. grade 25, Swiss Jewel Company, PA, USA) were self-aligned on the silicon carrier and bonded with Stycast 2850 epoxy.

The wear during batch-mode μUSM for tool spheres made of stainless steel 440 (SS440) and stainless steel (SS316) was compared by machining assembled N-BK7 spheres. The volume of the tool that was worn away was estimated from the change in height of the tool spheres. This change in height was measured by a laser displacement sensor (Keyence LKGD500, IL, USA). Table 3 lists the comparison of the wear in SS440 and SS316 spheres. Tool wear for SS440 was less than one-sixth as that of SS316. Hence SS440 spheres were used in the fabrication process.

After the workpiece spheres were assembled on the silicon carrier, lapping was performed using abrasive slurry (containing diamond particles with <0.25 μm diameter) to

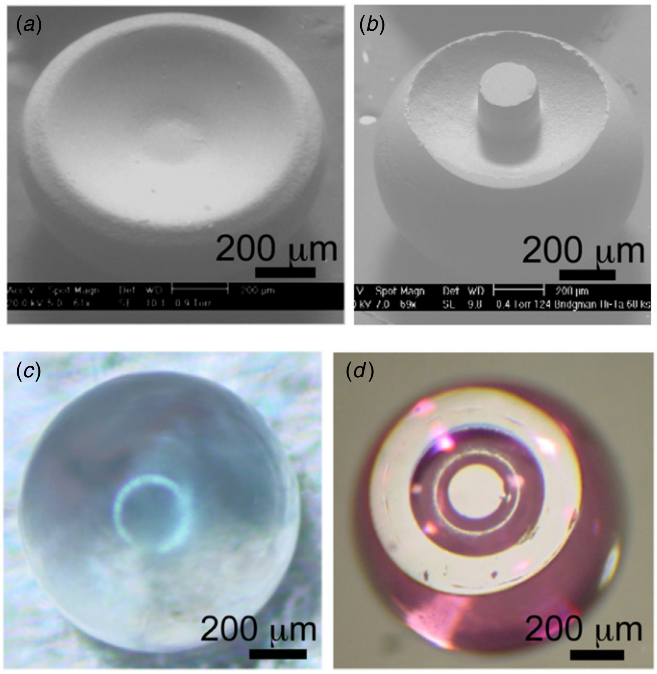

Figure 4. SEM images of the fabricated (*a*) concave spherical structure and (*b*) mushroom-shaped structure. (*c*) Photo of the top view of the mushroom structure made from transparent N-BK7 glass spheres. (*d*) Photo of a mushroom structure fabricated from a ruby sphere.

remove the excess epoxy, and in some cases to reduce the height of the workpiece spheres. A copper lapping plate was used in this process. A second batch-mode μUSM step was performed using the same parameters as listed in table 2. The spheres were then released using Dynasolve® 165 (Dynaloy, OH, USA), which is an effective solvent for the Stycast epoxy. Figures 4(*a*) and (*b*) show the SEM images of the fabricated concave and the mushroom-shaped spherical glass structures. The photograph of the outer surface of a mushroom structure fabricated from a 1 mm diameter N-BK7 glass sphere is shown in figure 4(*c*). A machining rate of 24 μm min^{-1} was achieved for a machining depth of 350 μm.

The feasibility of machining ruby spheres using the 3D-SOULE process was also verified. Ruby spheres of 1 mm outer diameter and 0.625 sphericity (A.F.B.M.A. grade 25, Swiss Jewel Company, PA, USA) were used in these experiments. Figure 4(*d*) shows the photograph of a fabricated mushroom structure from a ruby sphere. A machining rate of 12 μm min^{-1} was achieved for a machining depth of 50 μm with the same machining conditions as listed in table 2. The decrease in the machining rate from that of the N-BK7 spheres qualitatively matches to expectation based on equation (1), although there is a discrepancy in the ratio of the decrease.

The roughness (R_a) of the machined surfaces on N-BK7, ruby and silicon was measured using an Olympus LEXT OLS4000 laser interferometer. The results are shown in table 1 and plotted in figure 5. The surface roughness of Macor® ceramic, which was machined under the same machining conditions, is also included for reference [21]. As indicated by the dashed line in the figure, an approximate linear relationship can be observed between the surface roughness (R_a) and the product $K_{\mathrm{IC}}^{3/2}H^{1/2}$. This is consistent to the results shown in [26].

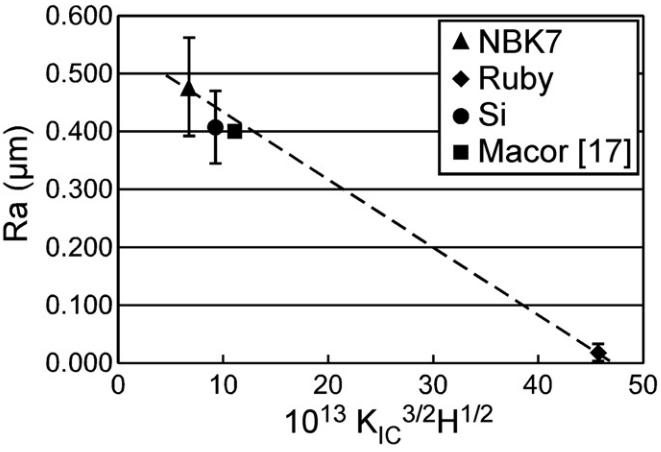

Figure 5. Relationship between the measured roughness (R_a) of the machined surface and the material constant ($K_{\mathrm{IC}}^{3/2}H^{1/2}$). Values for N-BK7 glass, ruby and Si are plotted. The values for Macor® glass-mica ceramic are also included for comparison [21]. The particles used for μUSM are WC powder of 0.5–1 μm size. The dashed line represents a linear relationship. The error bars indicate one standard deviation from the mean values ($n = 10$).

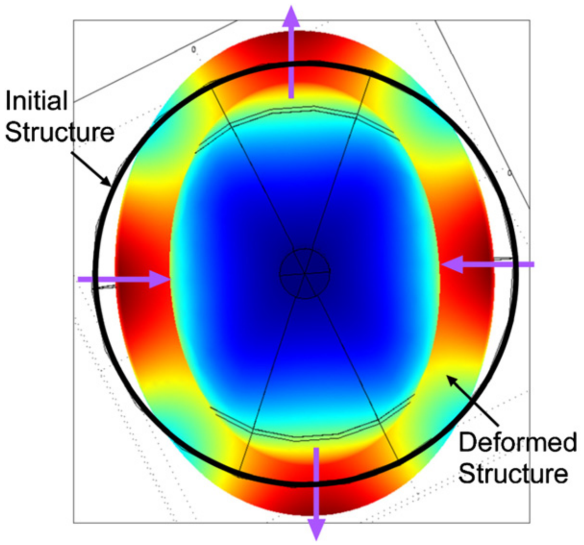

Figure 6. Simulated mode shape of the four-node 'wine-glass' resonance mode. The simulated and the experimentally measured values of the resonance frequency were 1.360 and 1.379 MHz, respectively.

3.2. Preliminary resonance characterization of mushroom structures

Finite element simulations were performed in order to estimate the resonance frequency of the fabricated structures. Eigenfrequency analysis was carried out on the N-BK7 mushroom-shaped structure with the fixed boundary condition applied to the stem of the structure. The diameter of the stem was 200 μm and the machining depth was assumed to be 250 μm. Figure 6 shows the simulated mode shape of the four-node

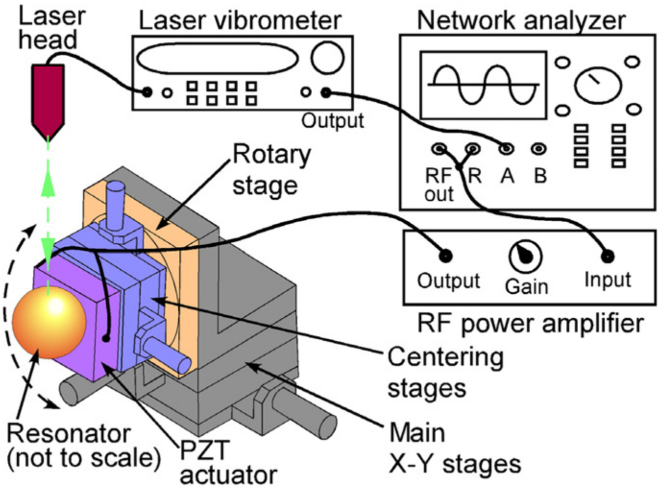

Figure 7. Setup used for resonance characterization of the micromachined resonators. The Polytec OFV3001S laser vibrometer was used to measure the vibration velocity of the resonators. The rotary stage, along with adjustment allowed by the main *X*–*Y* stages and the centering stages, enabled measurements along the circumference of the resonators. The Agilent 4395A network analyzer was connected to an RF power amplifier to sweep the frequency of the driving signal for the PZT actuator, and also to receive output from the laser vibrometer.

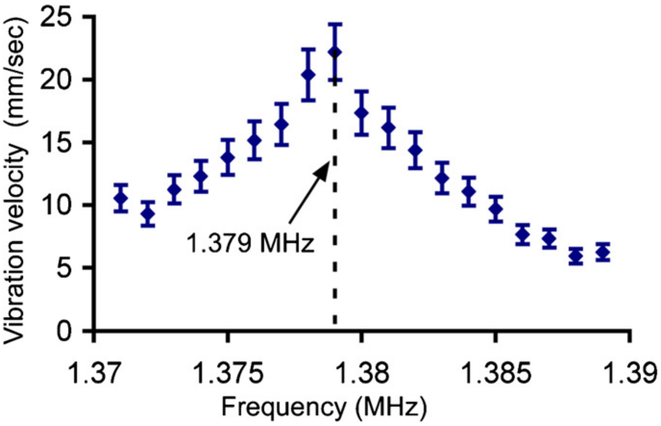

Figure 8. Resonance characteristics of the mushroom-shaped structure around the four-node wine-glass mode frequency (1.379 MHz) in air.

'wine-glass' resonance mode in the mushroom structure. It consists of four anti-nodes of maximum displacement and four-nodes of minimum displacement. This mode is selected for characterization as it is expected to have low anchor loss. Simulations suggest that the resonance frequency of this mode is 1.36 MHz.

The setup used for the resonance characterization of the machined mushroom-shaped structures is illustrated in figure 7. The mushroom-shaped structure was actuated with a PZT stack actuator (5 mm × 5 mm × 2 mm, Physik Instrumente Inc.). The stem of the structure was bonded to the PZT through a small brass spacer using adhesive. The PZT was mounted on the high precision *XY* centering stages (CVI Melles Griot), which were attached to a rotary stage (Thorlabs RP01) to enable centering of the test structure to the axis of rotation of the rotary stage. This also enabled the measurement of the vibration characteristics along the circumference of the mushroom-shaped resonator in order to verify the resonance mode. The vibration velocity of the mushroom-shaped structures was measured using a laser vibrometer (Polytec OFV3001S). The outer surface of the structure was coated with a thin layer of sputtered Cr/Au (20 nm/150 nm) in order to provide a surface with adequate reflection for the laser vibrometer. An Agilent 4395A network analyzer was connected to a power amplifier to sweep the frequency of the driving signal for the PZT, and also used to receive the corresponding output from the laser vibrometer.

Figure 8 shows the measured variation in the vibration velocity at a node on one of the mushroom structures as a function of the driving frequency. The resonance frequency of the 'wine-glass' mode was 1.379 MHz. The 'wine-glass' mode shape was confirmed by the measured vibration velocity at this resonance frequency along the circumference of the structure. This matches the simulation results described above. The quality factor of this resonance mode was measured to be 345 in air. This preliminary resonance characterization of the machined structures confirms the feasibility of using these as resonators.

4. Discussion

This work showed that spheres of N-BK7 glass and ruby can be successfully micromachined in batch mode using the 3D-SOULE process. Considering the characteristics of the μUSM process, other materials of interest can also be machined. For example, fused silica, which is favored for high *Q* resonators, has relevant material properties (K_{IC} and *H*) that are typically more amenable to USM than those of N-BK7. It is expected that the process can be applied to fused silica, and this will be investigated in future efforts.

As shown in table 3, a wear ratio of <5% was observed for tools made from SS440 for the μUSM step in the 3D-SOULE process, reducing from >30% tool wear with SS316. A highly wear-resistant tool material will further reduce the tool wear. For example, sintered polycrystalline diamond (PCD) tools, which can be shaped with the μEDM technique, are high wear-resistant and reported to provide 30–150 × improvement in tool wear over traditional tool materials such as WC and hard steels [27, 28].

Surface finish is important to achieve high quality factor of a resonator. As described in section 2, roughness of the machined surface is affected by a number of machining parameters. When other parameters remain the same, a finer abrasive can effectively reduce the surface roughness [20]. A surface roughness S_a of 5 nm has been demonstrated using 0.1 μm diamond abrasive [29], though the material removal rate will be reduced as well. A two-step μUSM can be performed to address this: a first step with larger abrasive size to remove the majority of the volume, and a second step using ultrafine diamond abrasive to improve the surface finish. In order to further improve the surface finish, chemical vapor polishing or other polishing techniques can be applied.

5. Conclusions

A 3D micromachining process combining batch-mode μUSM, lapping and μEDM for fabrication of concave and mushroom-shaped spherical structures was described. This process was demonstrated by machining spherical structures from materials including glass and ruby. Stainless steel 440 was determined to be the suitable tool material for μUSM and provided a tool wear ratio <5%. A machining rate of 24 μm sec^{-1} was achieved for fabrication of concave and mushroom-shaped spherical structures from 1 mm diameter N-BK7 glass spheres. Preliminary resonance characterization of the machined mushroom-shaped structures confirms the feasibility to use these as resonators. This process bears significant promise in the long term for wafer-scale microfabrication of spherical structures from high Q materials such as fused quartz.

Acknowledgments

The authors thank Prof. Karl Grosh and Katherine Kingsley for their help with the experiments using laser vibrometer. This work was supported in part by Defense Advanced Research Projects Agency (DARPA) under contract number W31P4Q-11-1-0002.

References

[1] Matthews A and Rybak F J 1992 Comparison of hemispherical resonator gyro and optical gyros *IEEE Aerosp. Electron. Syst. Mag.* **7** 40–6

[2] Shkel A M, Acar C and Painter C 2005 Two types of micromachined vibratory gyroscopes *IEEE Sensors Conf. (Irvine, CA)* pp 531–6

[3] Izmailov E A, Kolesnik M M, Osipov A M. and Akimov A V 1999 Hemispherical resonator gyro technology: problems and possible ways of their solutions *RTO SCI Int. Conf. on Integrated Navigation Systems (St. Petersburg, Russia)* pp 6-1–6-9

[4] Wu M C, Solgaard O and Ford J E 2006 Optical MEMS for lightwave communication *J. Lightwave Technol.* **24** 4433–54

[5] Becker E W, Ehrfeld W, Hagmann P, Maner A and Münchmeyer D 1986 Fabrication of microstructures with high aspect ratios and great structural heights by synchrotron radiation lithography, galvanoforming, and plastic moulding (LIGA process) *Microelectron. Eng.* **4** 35–56

[6] Guckel H 1998 High-aspect-ratio micromachining via deep x-ray lithography *Proc. IEEE* **86** 1586–93

[7] Douglas M A 1988 Trench etch process for a single-wafer RIE dry etch reactor *US Patent* No. 4,784,720

[8] Chou T K A and Najafi K 2002 Fabrication of out-of-plane curved surfaces in Si by utilizing RIE lag *MEMS'02: Proc. IEEE Int. Conf. Micro Electro Mechanical Systems (Las Vegas, NV)* pp 145–8

[9] Wise K D, Robinson M G and Hillegas W J 1981 Solid-state processes to produce hemispherical components for inertial fusion targets *J. Vac. Sci. Technol.* **18** 1179–82

[10] Sorenson L D, Gao X and Ayazi F 2012 3-D micromachined hemispherical shell resonators with integrated capacitive transducers *MEMS'12: Proc. IEEE Int. Conf. Micro Electro Mechanical Systems* pp 168–71

[11] Sorenson L D, Shao P and Ayazi F 2013 Effect of thickness anisotropy on degenerate modes in oxide micro-hemispherical shell resonators *MEMS'13: Proc. IEEE Int. Conf. Micro Electro Mechanical Systems* pp 169–72

[12] Zalalutdinov M, Aubin K L, Reichenbach R B, Zehnder A T, Houston B, Parpia J M and Craighead H G 2003 Shell-type micromechanical actuator and resonator *Appl. Phys. Lett.* **83** 3815–7

[13] Xie Y, Hsieh H-C, Pai P, Kim H, Tabib-Azar M and Mastrangelo C H 2012 Precision curved micro hemispherical resonator shells fabricated by poached-egg micro-molding *IEEE Sensors 2012 Conf. (Taipei)* pp 1–4

[14] Chan M L, Fonda P, Reyes C, Xie J, Najar H, Lin L, Yamazaki K and Horsley D A 2012 Micromachining 3D hemispherical features in silicon via micro-EDM *MEMS'12: Proc. IEEE Int. Conf. Micro Electro Mechanical Systems (Paris)* pp 289–92

[15] Sarac B, Kumar G, Hodges T, Ding S, Desai A and Schroers J 2011 Three-dimensional shell fabrication using blow molding of bulk metallic glass *J. Microelectromech. Syst.* **20** 28–36

[16] Prikhodko I P, Zotov S A, Trusov A A and Shkel A M 2011 Microscale glass-blown three-dimensional spherical shell resonators *J. Microelectromech. Syst.* **20** 691–701

[17] Senkal D, Ahamed M J, Trusov A A and Shkel A M 2013 High temperature micro-glassblowing process demonstrated on fused quartz and ULE TSG *Sensors Actuators* A **201** 525–31

[18] Cho J, Yan J, Gregory J A, Eberhart H, Peterson R L and Najafi K 2013 High-Q fused silica birdbath and hemispherical 3-D resonators made by blow torch molding *MEMS'13: Proc. IEEE Int. Conf. Micro Electro Mechanical Systems (Taipei)* pp 177–80

[19] Visvanathan K, Li T and Gianchandani Y B 2011 3D-SOULE: a fabrication process for large scale integration and micromachining of spherical structures *MEMS'11: Proc. IEEE Int. Conf. Micro Electro Mechanical Systems* pp 45–8

[20] Thoe T B, Aspinwall D K and Wise M LH 1998 Review on ultrasonic machining *Int. J. Mach. Tools Manuf.* **38** 239–55

[21] Li T and Gianchandani Y B 2006 A micromachining process for die-scale pattern transfer in ceramics and its application to bulk piezoelectric actuators *J. Microelectromech. Syst.* **15** 605–12

[22] Li T and Gianchandani Y B 2010 A high-speed batch-mode ultrasonic machining technology for multi-level quartz crystal microstructures *MEMS'10: Proc. IEEE Int. Conf. Micro Electro Mechanical Systems (Hong Kong)* pp 348–51

[23] Li T, Bai Q and Gianchandani Y B 2013 High precision batch mode micro-electro-discharge machining of metal alloys using DRIE silicon as a cutting tool *J. Micromech. Microeng.* **23** 095026

[24] Sun X-Q, Masuzawa T and Fujino M 1996 Micro ultrasonic machining and its applications in MEMS *Sensors Actuators* A **57** 159–64

[25] Komaraiah M and Reddy P N 1993 A study on the influence of workpiece properties in ultrasonic machining *Int. J. Mach. Tools Manuf.* **33** 495–505

[26] Guzzo P L, Raslan A A and De Mello J D B 1999 Relationship between quartz crystal orientation and the surface quality obtained by ultrasonic machining *Proc. 1999 Joint Meeting of the European Frequency and Time Forum (EFTF) and the IEEE Int. Frequency Control Symp. (IFCS) (Besancon, France)* pp 792–5

[27] Davis J R 1995 *Tool Materials* (Materials Park, OH: ASM International)

[28] Egashira K and Masuzawa T 1999 Microultrasonic machining by the application of workpiece vibration *CIRP Ann.: Manuf. Technol.* **48** 131–4

[29] Klopfstein M J, Ghisleni R, Lucca D A and Brinksmeier E 2008 Surface characteristics of micro-ultrasonically machined (1 0 0) silicon *Int. J. Mach. Tools Manuf.* **48** 473–6

[30] Swiss Jewel Company 2013 www.swissjewel.com/

[31] Boehly T R (ed) 1996 Surface microroughness of optical glasses under deterministic microgrinding *LLE Review* **66** 82–5

[32] Antunes J M, Cavaleiro A, Menezes L F, Simões M I and Fernandes J V 2002 Ultra-microhardness testing procedure with Vickers indenter *Surf. Coat. Technol.* **149** 27–35

[33] Roditi International Corporation 2013 *Laser Crystals* www.roditi.com/Laser/GenDescr.html

[34] Kyocera Industrial Ceramics Corporation 2013 http://americas.kyocera.com/kicc/industrial/crystal.html

[35] Scholz T, Schneider G A, Munoz-Saldana J and Swain M V 2004 Fracture toughness from submicron derived indentation cracks *Appl. Phys. Lett.* **84** 3055–7

[36] Anstis G R, Chantikul P, Lawn B R and Marshall D B 1981 A critical evaluation of indentation techniques for measuring fracture toughness: I, direct crack measurements *J. Am. Ceram. Soc.* **64** 533–8

[37] MatWeb 2012 *Material Property Data* www.matweb.com

[38] General Ruby and Sapphire Co. 2013 *Silicon* www.generalruby.com/Silicon.html

[39] Hopcroft M A, Nix W D and Kenny T W 2010 What is the Young’s modulus of silicon? *J. Microelectromech. Syst.* **19** 229–38

[40] Corning 2013 *Specialty Materials* www.corning.com/specialtymaterials/index.aspx

[41] Goodfellow Corporation 2013 www.goodfellow.com